Int. J. Electrochem. Sci., 15 **(2020)** 2511 – 2527, doi: 10.20964/2020.03.39

International Journal of
ELECTROCHEMICAL
SCIENCE
www.electrochemsci.org

Failure Behavior and Damage Mechanism of Acrylic Polyurethane Coating in Tropical Marine Atmospheric Environment

Zhao Li[1], *Jie Liu*[1,*], *Shaohua Xing*[2], *Lunwu Zhang*[3], *Zhonghai Lu*[1], *Peiqing Zhang*[1]

[1] College of Chemistry and Chemical Engineering, Yantai University, Yantai 264005, P. R. China
[2] State Key Laboratory for Marine Corrosion and Protection, Luoyang Ship Material Research Institute (LSMRI), Qingdao 266237, P. R. China
[3] Southwest Technology and Engineering Research Institute, Chongqing 400039, P. R. China
*E-mail: liujie6573@163.com

Received: 19 July 2019 / *Accepted:* 16 September 2019 / *Published:* 10 February 2020

Acrylic polyurethane coating was exposed to the tropical marine atmospheric environment for 24 months, and the physical, chemical and protective properties of the coating were investigated. The results demonstrated that the appearance, adhesion and protective property of the coating were degraded rapidly in the early exposure stage, and then changed slowly in the late exposure stage. During the filed exposure test, the ultraviolet irradiation was a major contributor to polyurethane chain scission of the coating, and the chain scission was mainly characterized by the rupture of C-N bonds. Moreover, the thermal stability of the coating was less affected by the tropical marine atmospheric environment.

Keywords: marine atmosphere; acrylic polyurethane coating; physical changes; chemical structures; EIS

1. INTRODUCTION

Acrylic polyurethane coating is used widely in automobiles, ships and spacecrafts due to its outstanding characteristics, including good weathering durability, excellent physical, chemical and mechanical properties [1-4]. However, the acrylic polyurethane coating used in outdoor conditions is susceptible to the external environment factors such as sunlight, temperature, moisture, oxygen, ozone, pollutants, etc., which can deteriorate its anticorrosion properties [5,6].

Since the relatively reliable experimental data can be obtained in a short period by applying accelerated ageing tests, scholars at home and abroad have studied the failure mechanism of organic coatings from photodegradation, thermal oxidative aging, oxidation degradation and so on, using various accelerated ageing tests [7-9]. For instance, by using thermal cycling test, Fedrizzi [10] reported that the water permeation caused damage to molecular structure of the organic coatings, which reduced the adhesion of the coating to substrate obviously. Hu and his coworkers [11] evaluated the failure process of acrylic polyurethane coating in artificial ultraviolet/condensation weathering environment, the results demonstrated that the xenon lamp exposure conditions affect the coating thickness and gloss significantly, while the changes of color difference and impendence of the coating confirmed a greater coating degradation under UV exposure conditions. However, accelerated ageing tests only take into account one or several major environmental factors, and the comprehensive effects of natural environmental factors on the coating performance cannot be truly reflected [12,13].

It has been acknowledged that the natural ageing tests are the most reliable methods to understand the long-term ageing performance of coating in actual service environment, although the test periods usually last for several years or even longer to obtain the failure information of samples [14-16]. As far as we know, few studies on the failure behavior and mechanism of acrylic polyurethane coating in natural marine atmosphere were reported up to now.

In this paper, the failure behavior and damage mechanism of acrylic polyurethane coating exposed to tropical marine atmospheric environment were characterized by various methods. The spectrophotometer, glossmeter, and scanning electron microscope (SEM) were applied to monitor the surface appearance and morphology of the coating. The coating adhesion was measured by the Pull-off test. ATR-FTIR and XPS techniques were applied to detect the chemical changes of the coating. The thermal stability and surface hydrophobicity were evaluated by thermal gravimetric analysis (TGA) and contact-angel measurement, respectively. Furthermore, the protective property of the coating was analyzed by electrochemical impedance spectroscopy (EIS).

2. EXPERIMENTAL

2.1 Materials

For sample preparation, cold rolled steel plates (100 mm×75 mm×2 mm) were used as the substrate. The substrates were polished with #1000 abrasive papers and cleaned with deionised water and ethanol. The acrylic polyurethane coating used in this paper was supplied by Feijing New Material Limited Company of China. The coating was applied by spray painting and cured at room temperature for 7 days, and the film thickness was in a range of 80±2 μm.

2.2 Field exposure test

The exposure site of this natural exposure test was located in Wanning, Hainan Province, China. The coated samples were placed facing south with an angle of 45°. The characteristics of atmospheric environment of Wanning in 2016 were shown in Table 1.

Table 1. Characteristics of atmospheric environment of Wanning in 2016

Environmental Characteristics	Average
Temperature (°C)	25.2
Relative humidity (%)	85.0
Precipitation (mm)	1647.0
Sunshine time (h)	1833.0
Chloride deposition deposition rate ($mg\cdot m^{-2}$)	8527
Sulfur oxide deposition rate ($mg\cdot m^{-2}$)	4965
NO_2 ($mg\cdot m^{-3}$)	0.005

2.3 Morphological observations

An EOS 750D digital camera (Canon Inc, Japan) was used to observe the macroscopic morphology of the coating surface. The microstructure of the coating surface was studied using a JSM-6480LV scanning electron microscope (Jeol Inc, Japan), with a 20 kV accelerating voltage.

2.4 Appearance characterizations

A Picogloss 503 glossmeter (Erichsen Inc, Germany) at a 60° incidence angle was used to measure the surface gloss values of the coating, and the surface color was measured using a 565 spectrophotometer (Erichsen Inc, Germany). The color difference ΔE could be calculated by the equation $\Delta E=\sqrt{(\Delta L)^2+(\Delta a)^2+(\Delta b)^2}$, where ΔL represented the lightness, Δa represented the relationship between green and red, and Δb reflects the relationship between blue and yellow. Each sample was measured 5 replicates to obtain averaged values.

2.5 Adhesion tests

According to ASTM D4541-2009 [17], the adhesion measurements were performed by a PosiTest AT-A adhesion tester (DeFelsko Inc, USA). Five parallel samples for each exposure time were conducted, and the results were reported as an average of the five measurements.

2.6 ATR-FTIR analysis

ATR-FTIR was carried out to study the degradation of the chemical composition and structure of the coating at room temperature (25 °C), using a Spectrum GX FTIR Spectrometer (PerkinElmer Inc., USA) equipped with a diamond ATR unit. The wavenumber range for ATR-FTIR measurements was 400 cm^{-1}-4000 cm^{-1}.

2.7 XPS analysis

XPS measurements were conducted by an AXIS Ultra XPS spectrometer (Kratos Inc, Britain), equipped with an achromatic Al Kα X-ray source. The survey scans were spanned from 0 eV to 1200 eV in 1 eV step. For the High-resolution spectra for C1s, the hydrocarbon component at 284.8 eV was used to correct the binding energies [18], and the XPS spectrum was fitted by XPS Peak 4.1 software.

2.8 Thermal gravimetric analysis (TGA)

TGA of the coating was performed with a STA449 F5 thermal analyzer (Netzsch Inc, Germany). Film samples (approximately 3-5 mg) were heated in a nitrogen atmosphere from 25 ℃ to 800 ℃, with a 10 $°C\cdot min^{-1}$ heating rate.

2.9 Contact-angle measurements

The wetting properties of the coating surface were determined in terms of contact-angle, using a JC2000D1 contact angle measuring instrument (Zhongchen Inc, China). 4 μL deionized water was used as the liquid and each sample was repeated 5 times for measurements to average. The values of contact-angle were calculated by the software that came with the instrument.

2.10 EIS measurements

EIS measurements were performed by CS310 potentiostat (Wuhan Corrtest Inc., China) in a three-electrode cell, with a test area of 7 cm^2 for each sample. The frequency range was 10^5-10^{-2} Hz and the perturbation voltage was set at 20 mV. A saturated calomel electrode (SCE) and a platinum wire (Φ 5 mm) were used as reference electrode and auxiliary electrode, respectively. The electrolyte solution for experiments was NaCl aqueous solution, with a mass fraction of 3.5%. The EIS data was analyzed via ZsimpWin software.

3. RESULTS AND DISCUSSION

3.1 Morphological observations

Fig. 1 presented the evolution of macro morphology of the samples exposed for various times. It could be seen obviously from Fig. 1(a) that the unaged coating surface was fairly homogeneous and smooth, with no visible defects. As the exposure time elapsed, the coating gradually faded, small blisters and yellow corrosion products could be seen at the edge area of the coating and the quantity and size of the blisters gradually increased. Besides, the signs of corrosion in carbon steel under the coating became more and more obvious. When exposed for 24 months, large area of the coating was peeled off from the metal substrate and the metal was severely corroded.

Figure 1. Macro morphology of the coating with different exposure cycles: (a) 0 month; (b) 6 months; (c) 12 months; (d) 24 months.

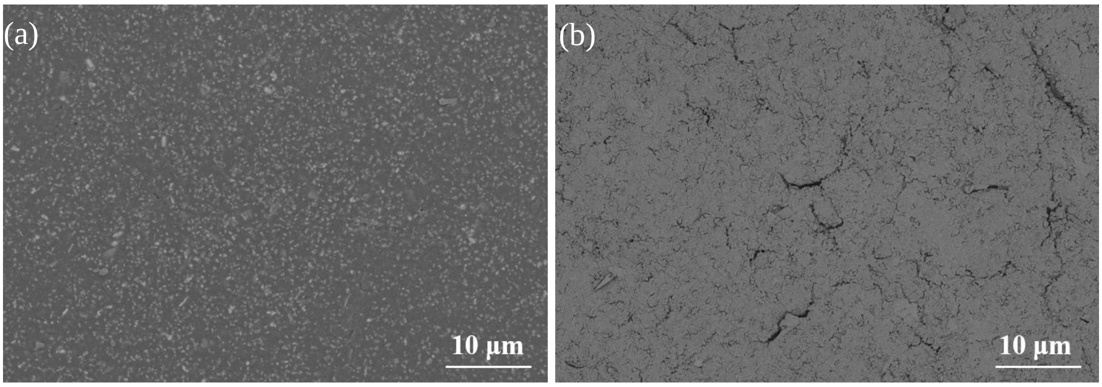

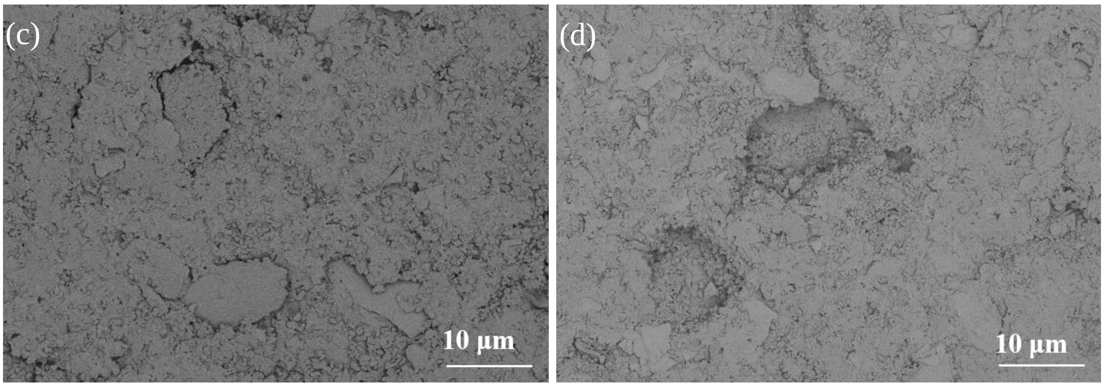

Figure 2. Micrographs of the coating with different exposure cycles: (a) 0 month; (b) 6 months; (c) 12 months; (d) 24 months.

The evolution of micro-morphology of acrylic polyurethane coating was shown in Fig. 2. The unaged coating surface remained smooth and no obvious defects were found, and the pigment particles were uniformly distributed in the resin. As shown in Fig. 2(b), when exposed for 6 months, the coating surface turned rough slightly and some cracks and voids appeared on the surface, which meant the smoothness of the coating surface was significantly reduced. After 12 months of exposure, the coating was deteriorated obviously and some pigment particles were exposed on the coating surface. The cracks and voids increased and became larger. After exposed for 24 months, there were more defects on the coating surface, and the paint film was damaged seriously, suggesting that the coating might lose its barrier property.

3.2 Change in appearance

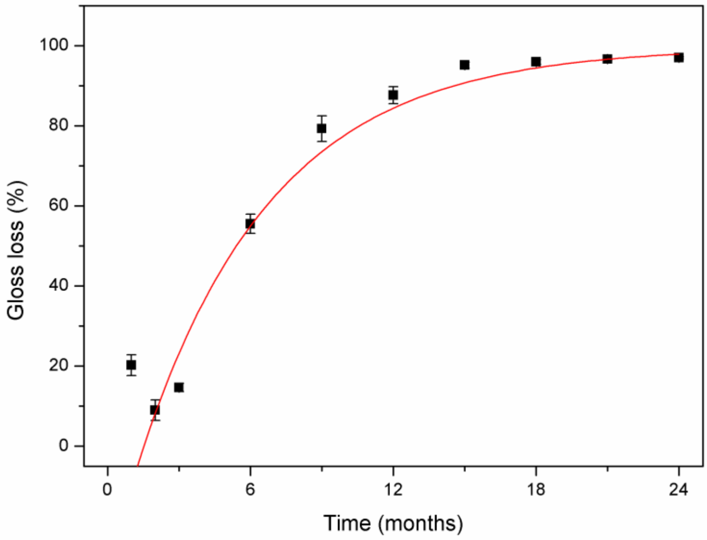

Figure 3. Gloss loss of the coating with different exposure cycles.

Fig. 3 displayed the changes of the gloss loss of acrylic polyurethane coating with different exposure times. It was seen clearly that the gloss loss increased exponentially as a function of exposure time, and the fitting equation was:

$$\Delta G=99.65-130.83\exp(t/-5.58)$$

where ΔG was the gloss loss, t was the exposure time and the correlation coefficient was 0.97. The curve in Fig. 3 exhibited two typical phases for the gloss loss with exposure time. The specular gloss loss increased to 87% rapidly during phase I (0-12 months). The reason for this phenomenon was that the strong ultraviolet radiation accelerated the degradation of the resin, which led to the obvious pore and wrinkle morphology on the coating surface [19,20]. The evolution of the micro-morphology of the coating also proved that the increasingly rough surface morphology and residual pigment particles were the main contributor for the gloss loss of the coating. In addition, the volatilization of solvents or other volatile materials inside the coating at the beginning of exposure also resulted in the unsmooth surface to some extent. It was worth noting that the gloss loss of the sample exposed for 2 months decreased slightly, which might be attributed to the release and redistribution of coating internal stress [21]. In phase II (12-24 months), the gloss loss entered a relative stable stage and eventually remained at around 95%, revealing a severe ageing of the coating exposed to tropical marine atmosphere for 24 months.

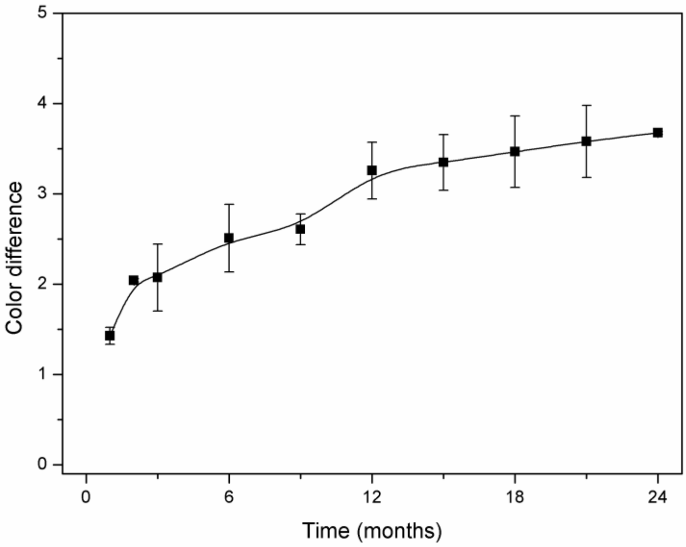

Figure 4. Color difference of the coating with different exposure cycles.

Fig. 4 illustrated the trend in color difference of the coating with exposure time. It was obvious that the color difference increased continuously during the exposure test. In fact, the value changes (0-3.25) in color difference within the period of 0-12 months was approximately eight times than that (3.25-3.67) of 12-24 months. The originally intact paint film of the coating was gradually destroyed in the first 12 months, causing the pigment particles to emerge from the resin matrix. That led to an obvious impact on the color difference of the coating. However, the increase of color difference during the second 12 months was mainly attributed to the slow degradation of residual resin between the pigment particles, so the color difference did not change too much [22].

From the above analysis, it was believed that the tropical marine atmospheric conditions affected the coating appearance significantly. The gloss loss and color difference of the coating showed a similar variation in the exposure test for 24 months, which were characterized by a rapid increase in the early stage and then remained almost unchanged in the following time.

3.3 Adhesion tests

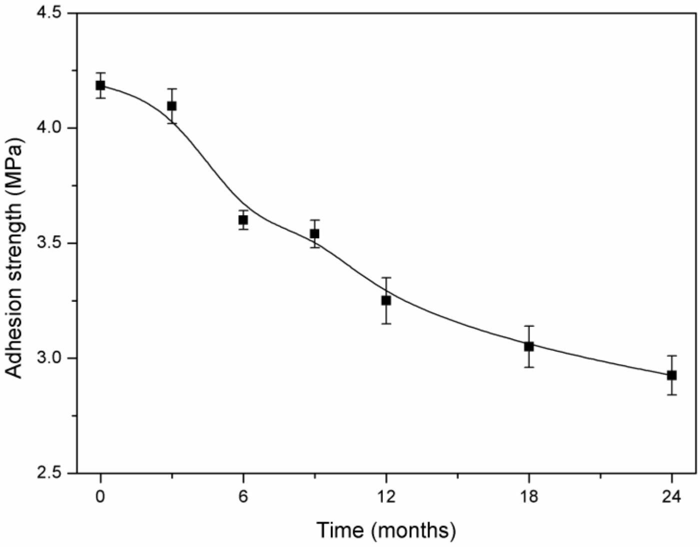

Figure 5. Coating adhesion with different exposure cycles.

The changes of coating adhesion during the exposure test were shown in Fig. 5. During the first and second 12 months, the coating adhesion decreased by 0.94 MPa and 0.33 MPa, respectively. According to the micro-morphology of the coating in Fig. 2, there were many cracks and voids on the coating surface, which made it easy for water molecules to accumulate and diffuse at the coating/metal interface. That caused the coating adhesion to decrease to some extent. Furthermore, the carbon steel substrate would be corroded, and the cathodic reaction was as follows:

$$O_2+2H_2O+4e^-\rightarrow 4OH^-$$

It has been reported widely that the accumulation of OH^- at the coating/metal interface further reduced the coating adhesion [23].

3.4 ATR-FTIR analysis

Chemical structure of acrylic polyurethane coating was given by ATR-FTIR, as shown in Fig. 6. For unaged coating, the peaks at 2935 cm^{-1} and 1378 cm^{-1} were assigned to the asymmetric stretching and bending vibration of $-CH_2$, respectively. A strong peak at 1729 cm^{-1} was the typical characteristic peak of C=O stretching vibration [24]. The peaks at 1640 cm^{-1} and 1521 cm^{-1} were determined by urethane (CNH) groups. The presence of bending vibration of $-CH_3$ was confirmed by the peaks at 1454 cm^{-1} and 2859 cm^{-1}. Two peaks at 1162 cm^{-1} and 1122 cm^{-1} were attributed to the C-O bonds. The characteristic peaks at 1070 cm^{-1} and 1027 cm^{-1} might be associated with the stretching vibration of S_i-O-S_i, which was related to pigments such as hydrated magnesium silicate [25].

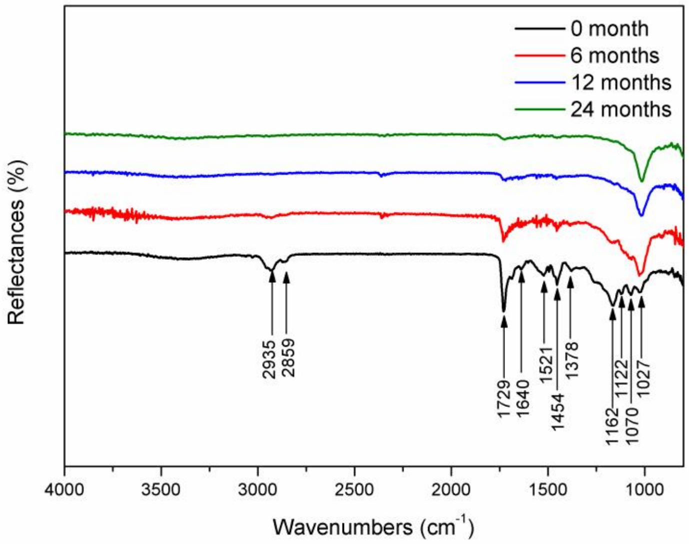

Figure 6. ATR-FTIR spectra of the coating with different exposure cycles.

As the exposure time increased, the intensities of the main absorption peaks were gradually decreased, while the absorption band representing the coating pigment increased significantly in intensity, which meant a lot of pigment particles were revealed on the coating surface due to the degradation of coating resin. After exposure for 24 months, it could be seen clearly from ATR-FTIR spectra that the characteristic peaks almost disappeared except for the peaks representing the pigment and C=O bonds, which meant the main functional groups of acrylic polyurethane coating were seriously destroyed.

Table 2. The corresponding relation between the polymer bond energy and wavelength

Chemical bond	Bond energy (kJ·mol^{-1})	Wavelength (nm)
C-H	413.66	290
N-H	391.05	306
C-O	351.69	340
C-N	290.98	400

As we all know, the sunlight shining on the ground was mainly composed of ultraviolet (280-400 nm), visible light (400-780 nm) and infrared (780-3000 nm). According to the polymer bond energy in Table 2, the ultraviolet radiation was strong enough to break many typical chemical bonds in polyurethane chain [26-28]. Notably, the C-N bonds were more easily broken as a result of the lower bond energy, which could be confirmed by the XPS analysis in the next section. Besides, based on the atmospheric environment characteristics in Wanning (in Table 1), the high humidity could also initiate hydrolysis of the hydrophilic ester and carbamate groups in the polyurethane chain, and this process could be accelerated by the high temperature [29].

3.5 XPS analysis

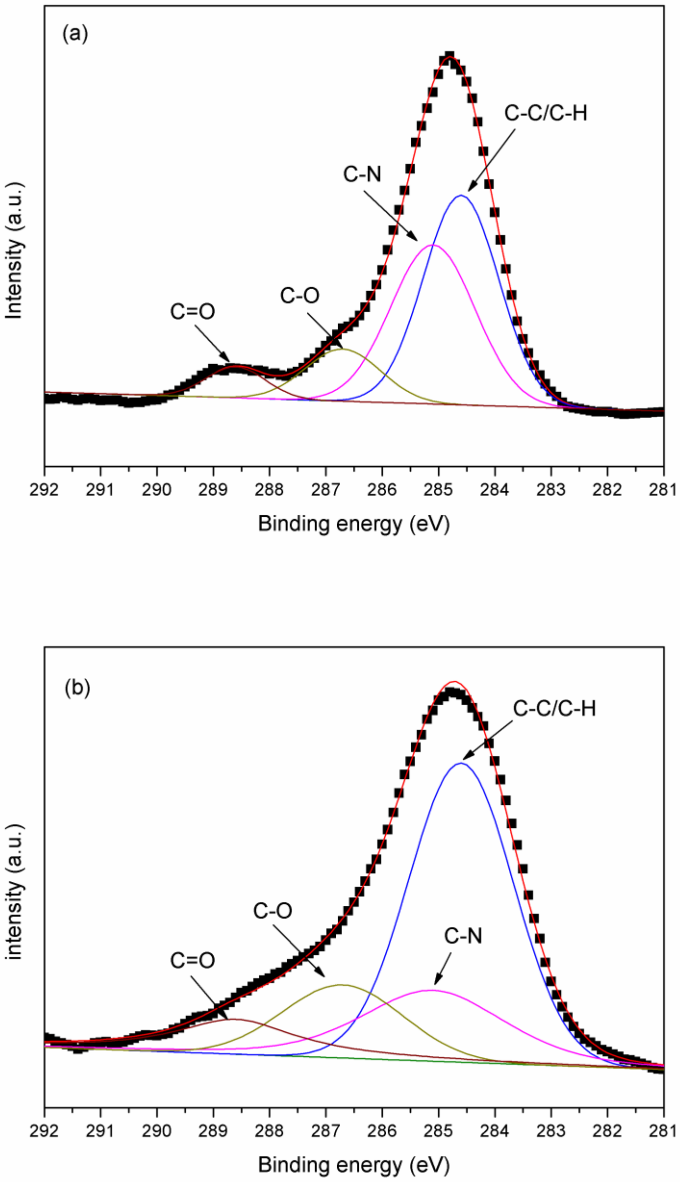

Figure 7. C1s spectrum of acrylic polyurethane coating at (a) 0 month and (b) 24 months of exposure.

Table 3. XPS results of C1s spectrum of acrylic polyurethane coating before and after exposure for 24 months

Exposure time (month)	Peak A (eV)	Structure	Peak B (eV)	Structure	Peak C (eV)	Structure	Peak D (eV)	Structure
0	284.6 (45.16%)	C-C/C-H	285.1 (38.32%)	C-N	286.7 (11.25%)	C-O	288.6 (5.27%)	C=O
24	284.6 (53.36%)	C-C/C-H	285.1 (20.65%)	C-N	286.7 (14.99%)	C-O	288.6 (11.00%)	C=O

Fig. 7 exhibited the C1s spectrum of the coating before and after exposure for 24 months. It could be found that there were four main peaks in the C1s spectrum, including C-C/C-H (284.6 eV), C-N (285.1 eV), C-O (286.7 eV) and C=O (288.6 eV) [30].

After 24 months of exposure, the relative proportions of carbon functional groups changed obviously compared with the unaged coating. The XPS results (Table 3) showed that the ratio of C-C/C-H, C-O and C=O bonds increased by 8.20%, 3.74% and 5.73%, respectively, while the ratio of C-N bonds decreased by 16.67%, which indicated that there was scission of C-N bonds. These results were in good agreement with ATR-FTIR analysis that the polyurethane main chain scission was mainly characterized by the rupture of C-N bonds.

3.6 Thermal stability analysis

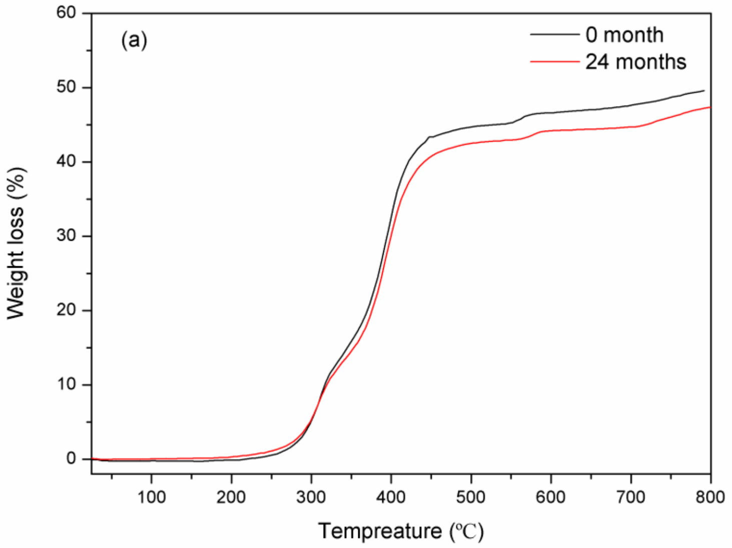

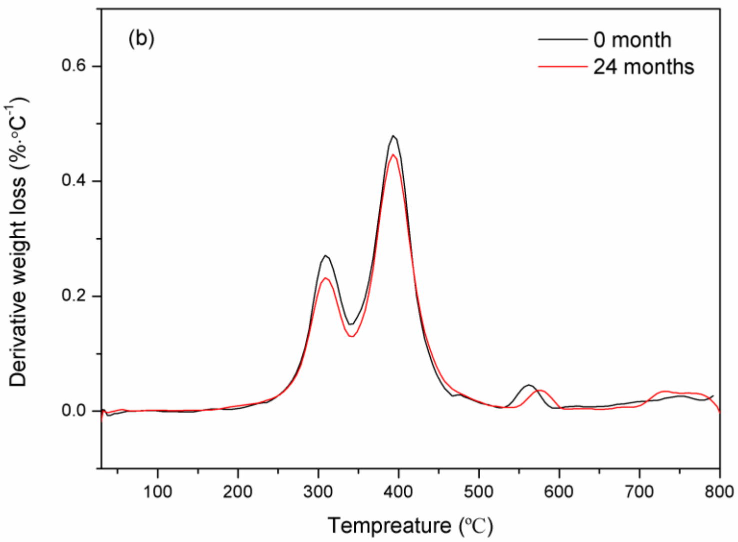

Figure 8. (a) TGA and (b) DTG curves of the coating before and after exposure for 24 months.

Table 4. The results of TGA of the acrylic polyurethane coating before and after exposure for 24 months

Exposure time (month)	T_{on1} (°C)	T_{max1} (°C)	Δw_1 (%)	T_{on2} (°C)	T_{max2} (°C)	Δw_2 (%)
0	158.78	313.36	15.56	346.43	397.69	31.07
24	152.23	308.35	13.93	348.37	392.78	30.07

As shown in Fig. 8, there were two main stages of thermal degradation for both unaged and aged coating, and an inconspicuous degradation stage could be seen during 525-610 °C, which was related to the carbonization of the residual samples [31]. The detailed thermal characteristics were summarized in Table 4, in which T_{on} represented the onset temperature of degradation, T_{max} was the temperature of maximum degradation rate, and Δw was the weight loss. In general, the thermal characteristics demonstrated that the thermal stability of acrylic polyurethane coating was less affected by the tropical marine atmospheric environment.

3.7 Contact-angel measurements

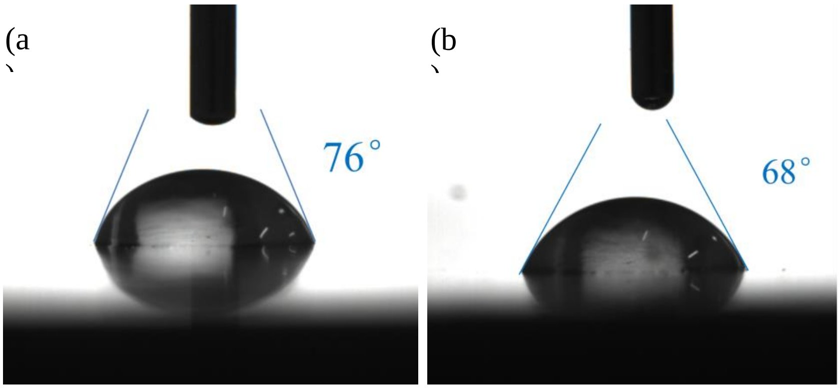

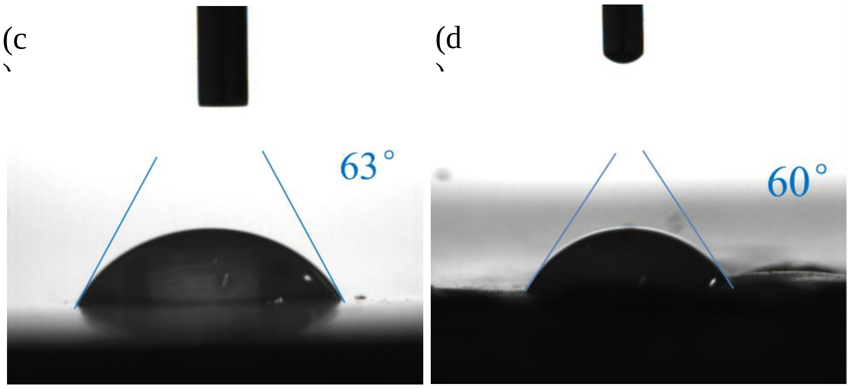

Figure 9. Water contact-angles of coating surface with different exposure cycles: (a) 0 month; (b) 6 months; (c) 12 months; (d) 24 months.

Surface wettability was closely related to the anticorrosive capability of coating and the contact-angle can reflect the wetness degree of the solid surface by the liquid [32]. Fig. 9(a) showed that the unaged coating surface was slightly hydrophilic as it contained some polar groups such as amino and carboxyl groups, with a water contact-angle of 76°. As the exposure time increased, the contact-angle gradually decreased, indicating that the hydrophilic of the coating surface was enhanced. The enhanced hydrophilic was mainly attributed to the increasingly rough coating surface [33], which facilitated the water penetration into the microstructures of the aged coating surface under gravity.

3.8 Protective property

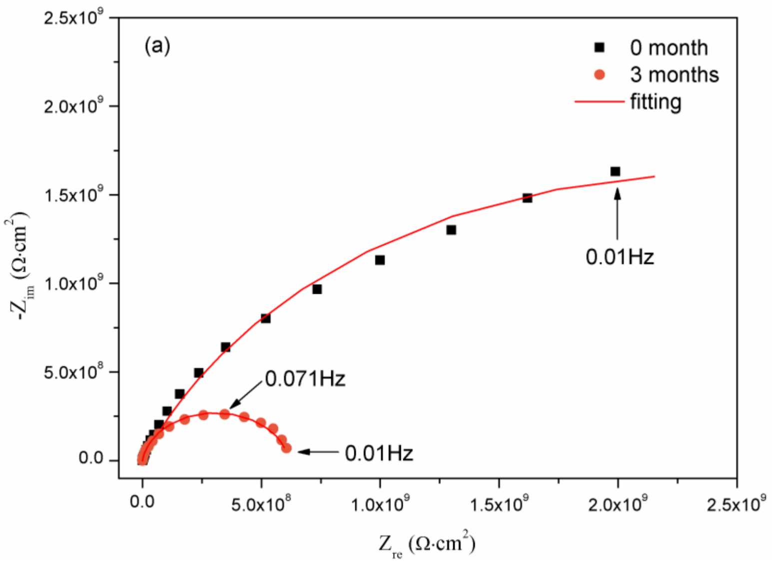

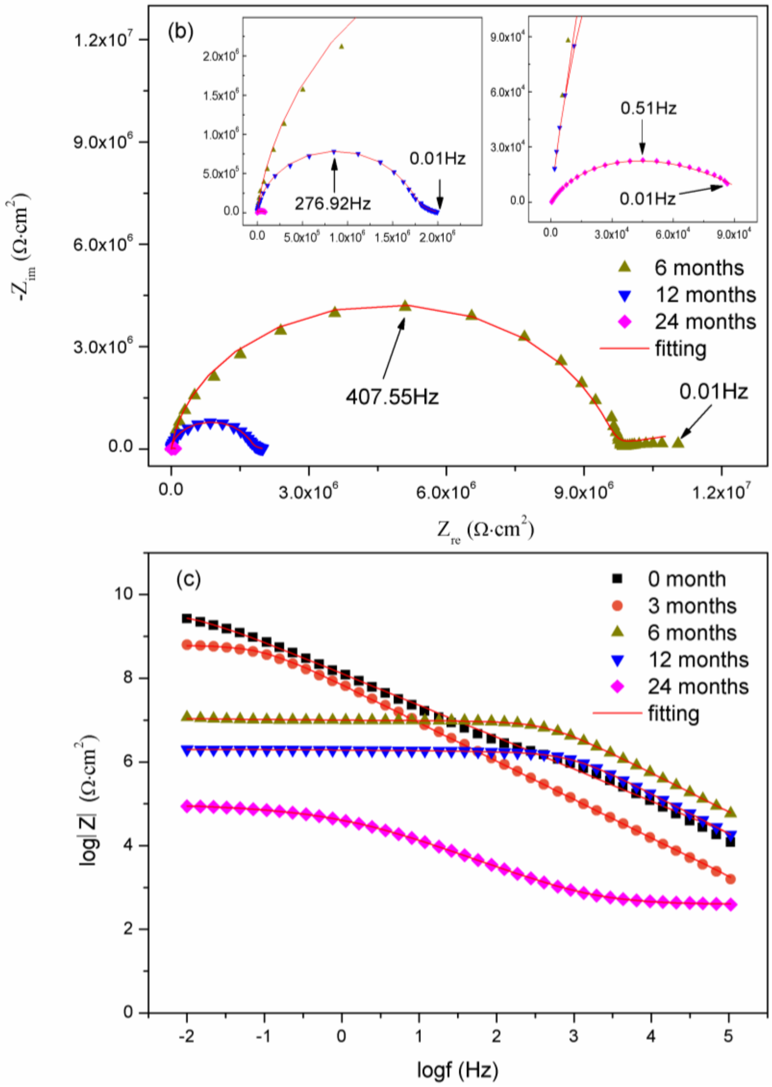

Figure 10. Nyquist and Bode plots and fitting results with different exposure cycles.

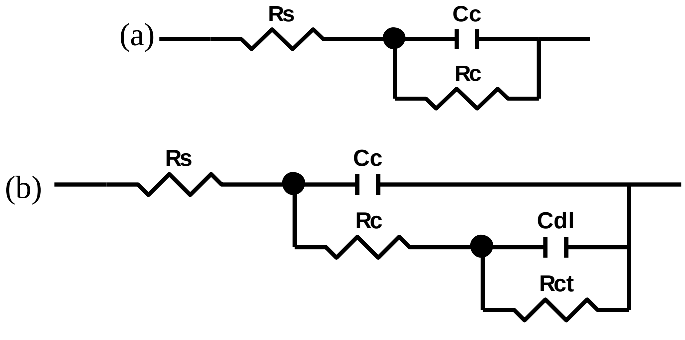

Figure 11. Electrical equivalent circuit model for EIS data fitting.

Table 5. The fitting results of electrochemical parameters of coated system with different exposure cycles

Exposure time (months)	R_c ($\Omega\cdot$cm^2)	Q_c (S$\cdot$s$^n\cdot$cm^{-2})	R_{ct} ($\Omega\cdot$cm^2)	Q_{dl} (S$\cdot$s$^n\cdot$cm^{-2})
0	4.69×10^9	1.86×10^{-9}	—	—
3	6.15×10^8	2.60×10^{-9}	—	—
6	9.06×10^6	6.48×10^{-7}	1.03×10^{10}	8.31×10^{-7}
12	1.58×10^6	7.64×10^{-7}	4.24×10^5	3.91×10^{-7}
24	5.07×10^4	3.60×10^{-6}	5.18×10^4	1.97×10^{-5}

Figure 10(a) and (b) were the Nyquist plots and fitting results of acrylic polyurethane coating for different exposure times, and the fitted results of electrochemical parameters were shown in Table 5. When fitting the EIS data, the pure capacitance was replaced by the constant phase element (CPE) to eliminate the influence of the non-ideal behavior of the coating on fitting results [34]. Therefore, the fitting data were obtained as CPE, but was referred to as capacitance for simplicity. The Nyquist diagram for unaged coating appeared as a single capacitive loop corresponding to one time constant [35]. The EIS data at this stage was fitted using the electrical equivalent circuit (EEC) in Fig. 11(a). R_s was the solution resistance, R_c and C_c denoted coating resistance and coating capacitance, respectively. For unaged acrylic polyurethane coating, the coating resistance (R_c) was 4.69×10^9 $\Omega\cdot$cm^2, and thus it was believed that the coating was a intact shield layer [36]. After exposure for 3 months, due to the water uptake of the coating, the amount of R_c decreased while C_c increased, revealing that the barrier property of the coating was gradually reduced. During this period, the EIS data was still matched well with the EEC in Fig. 11(a).

As shown in Fig. 10(b), in the case of the coating exposed for 6-24 months, the selected EEC for EIS data was depicted in Fig. 11(b), where C_{dl} and R_{ct} represented the double-layer capacitance and charge-transfer resistance, respectively. With the exposure time going on, the capacitive loop in high frequency was further decreased, and the second capacitive loop could be seen in the low frequency range, which meant the electrolyte had reached the metal surface and the electrochemical reactions at the coating/metal interface had begun [37,38]. It was noteworthy that there was only one capacitive loop could be seen in the Nyquist plots of the coating exposed for 24 months. The explanation for the phenomenon might be that the magnitude of the capacitive loop representing the electrochemical reaction was close to that of the coating's physical impedance [39]. Obviously, the values of R_c and R_{ct} continued to decrease, especially the R_c of the coating exposed for 24 months was below 10^6 $\Omega\cdot$cm^2, which could be considered as losing the protective property [40,41].

Futhermore, the Bode plots (Fig. 10c) clearly displayed the changes of impedance modulus (|Z|) of the coating during the field exposure test. The amount of the $|Z|_{0.01\ \mathrm{Hz}}$ decreased sharply from 9.42×10^9 $\Omega\cdot$cm^2 to 6.29×10^6 $\Omega\cdot$cm^2 in the first 12 months, which was corresponded to the rapid change of the appearance and adhesion of the coating in the early exposure stage. The structure of the coating at this stage was seriously injured from the surface to the inner. In the second 12 months, the coating had been severely aged and was almost completely failed. Therefore, the amount of $|Z|_{0.01\ \mathrm{Hz}}$ was only decreased from 6.29×10^6 $\Omega\cdot$cm^2 to 4.93×10^5 $\Omega\cdot$cm^2, and the appearance and adhesion of the coated sample did not change obviously.

4. CONCLUSIONS

From the systematic investigation of the failure behavior and damage mechanism of acrylic polyurethane coating exposed to tropical marine atmospheric environment for 24 months, it could be demonstrated that, the appearance, adhesion and protective property of the coating were deteriorated rapidly in the early stage of exposure, and then changed slowly in the late stage of exposure. During the field exposure, the ultraviolet irradiation was an important cause of polyurethane chain scission of the coating, and the chain scission was mainly characterized by the rupture of C-N bonds. In addition, the tropical marine atmospheric conditions did not significantly affect the thermal stability of the coating.

ACKNOWLEDGMENTS

This work was supported by National Natural Science Foundation of China (No. 51971192); Equipment Development Department and China Shipbuilding Industry Corporation unite foundation (No. 6141B04080206); National Defense Technology Foundation (No. JSHS2015209C003 & JSHS2015209B001); Graduate Innovation Foundation of Yantai University (GIFYTU) (No. YDZD1912).

References

1. F. Dolatzadeh, M.M. Jalili and S. Moradian, *Mater. Corros.*, 64 (2013) 609.
2. V.V. Gite, P.P. Mahulikar and D.G. Hundiwale, *Prog. Org. Coat.*, 68 (2010) 307.
3. J. Zhao, T. Zhou, J.H. Zhang, H.M. Chen, C.Y. Yuan, W.D. Zhang and A.M. Zhang, *Ind. Eng. Chem. Res.*, 53 (2014) 19257.
4. J. Weiss, M. Voigt, C. Kunze, J.E. Huacuja Sánchez, W. Possart and G. Grundmeier, *Int. J. Adhes. Adhes.*, 70 (2016) 167.
5. J. Liu, X. B. Li, L. K. Xu and P. Q. Zhang, *Polym. Test.*, 54 (2016) 59.
6. H. Katayama and S. Kuroda, *Corros. Sci.*, 76 (2013) 35.
7. F.X. Perrin, M. Irigoyen, E. Aragon and J.L. Vernet, *Polym. Degrad. Stab.*, 72 (2001) 115.
8. D. Santos, A. Soares Vieira and E. Almeida, *Mater. Corros.*, 51 (2000) 481.
9. X.F. Yang, D.E. Tallman, G.P. Bierwagen, S.G. Croll and S. Rohlik, *Polym. Degrad. Stab.*, 77 (2002) 103.
10. L. Fedrizzi, A. Bergo, F. Deflorian and L. Valentinelli, *Prog. Org. Coat.*, 48 (2003) 271.
11. J.W. Hu, X.G. Li, J. Gao and Q.L. Zhao, *Prog. Org. Coat.*, 65 (2009) 504.
12. S. Amrollahi, M. Mohseni and B. Ramezanzadeh, *Prog. Org. Coat.*, 105 (2017) 132.
13. A. Miszczyk and K. Darowicki, *Corros. Sci.*, 43 (2001) 1337.
14. B. Wang, X.B. Li, J. Liu and H. Jiang, *Mater. Corros.*, 69 (2018) 888.
15. M. Kohl and A. Kalendová, *Prog. Org. Coat.*, 86 (2015) 96.
16. S. Zhang, Y.T. He, T. Zhang, G.R. Wang and X. Du, *Mater.*, 11 (2018) 965.
17. ASTM D 4541-02, 2002 Standard Test for Pull-off Strength of Coatings using Portable Adhesion Testers. *ASTM International, West Conshohocken, PA*.
18. G.Y. Cai, D.P. Zhang, D. Jiang and Z.H. Dong, *Prog. Org. Coat.*, 124 (2018) 25.
19. X.F. Yang, C. Vang, D.E. Tallman, G.P. Bierwagen, S.G. Croll and S. Rohlik. *Polym. Degrad. Stab.*, 74 (2001) 341.
20. G. Theiler, V. Wachtendorf, A. Elert and S. Weidner, *Polym. Test.*, 70 (2018) 467.
21. J.W. Hu, X.G. Li, J. Gao and Q.L. Zhao, *Prog. Org. Coat.*, 65 (2009) 504.

22. G. Gheno, R. Ganzerla, M. Bortoluzzi and R. Paganica, *Prog. Org. Coat.*, 101 (2016) 90.
23. A. Leng, H. Streckel, K. Hofmann and M. Stratmann, *Corros. Sci.*, 41 (1998) 599.
24. M. Rashvand and Z. Ranjbar, *Mater. Corros.*, 65 (2014) 76.
25. Y. Su, C. Shu, L.Z. Luo and H. Su, *Surf. Technol.*, 40 (2011) 18.
26. M. Fratricova, P. Simon, P. Schwarzer and H.W. Wilde, *Polym. Degrad. Stab.*, 91 (2006) 94.
27. M. Ifigoyen, E. Aragon, F.X. Perrin and J.L. Vernet, *Prog. Org. Coat.*, 59 (2007) 259.
28. J.Y. Charmeau and E. Kientz, *Prog. Org. Coat.*, 27 (1996) 87.
29. T.V. Nguyen, X.H. Le, P.H. Dao, C. Decker and P. Nguyen-Tri, *Prog. Org. Coat.*, 124 (2018) 137.
30. G.Y. Cai, D.P. Zhang, D. Jiang and Z.H. Dong, *Prog. Org. Coat.*, 124 (2018) 25.
31. I.A. Wonnie Ma, A. Sh, K. Ramesh, B. Vengadaesvaran, S. Ramesh and A.K. Arof, *Prog. Org. Coat.*, 113 (2017) 74.
32. M. Shon and H. Kwon, *Corros. Sci.*, 51 (2009) 650.
33. D. Han, L. Zhu, Y Chen, W.P. Li and L.L Feng, *J. Fluorine. Chem.*, 156 (2013) 38.
34. J.M. Hu, J. Q. Zhang and C.N. Cao, *Prog. Org. Coat.*, 46 (2003) 273.
35. J. Liu, X.B. Li, J. Wang, T.Y. Luo and X.M. Wang, *Prog. Org. Coat.*, 76 (2013) 1075.
36. M.R. da Silveira, I.N. Ivancko, M.B. Valério, L.Y. Reznik, L.J. de Carvalho, A. da Costa Rodrigues and A.L.N. da Silva, *Polym. Test.*, 69 (2018) 410.
37. M. Bobby Kannan, R. Walter, A. Yamamoto, H. Khakbaz and C. Blawert, *RSC Adv.*, 8 (2018) 29189.
38. J. Liu, W. Wang and J. Wang, *Mater. Sci. Tech.*, 21 (2013) 33.
39. C.F. Zhu, R. Xie, J.H. Xue and L.L. Song, *Electrochim. Acta*, 56 (2011) 5828.
40. J.T. Zhang, J.M. Hu, J.Q. Zhang and C.N. Cao, *Prog.* Org. *Coat.*, 49 (2004) 293.
41. F. Yang, T. Liu, J.G. Li, S.H. Qiu and H.C. Zhao, *RSC. Adv.*, 8 (2018) 13237.

© 2020 The Authors. Published by ESG (www.electrochemsci.org). This article is an open access article distributed under the terms and conditions of the Creative Commons Attribution license (http://creativecommons.org/licenses/by/4.0/).